

FineXtrol: Controllable Motion Generation via Fine-Grained Text

Keming Shen^{1,2}, Bizhu Wu^{1,2,3}, Junliang Chen⁴, Xiaoqin Wang^{1,2}, Linlin Shen^{1,2,5*}

¹School of Computer Science and Software Engineering, Shenzhen University

²Guangdong Provincial Key Laboratory of Intelligent Information Processing, Shenzhen University

³School of Computer Science, University of Nottingham Ningbo China, Ningbo, China

⁴Department of Electrical and Electronic Engineering, The Hong Kong Polytechnic University

⁵Computer Vision Institute, School of Artificial Intelligence, Shenzhen University

2400101005@mails.szu.edu.cn, llshen@szu.edu.cn

Abstract

Recent works have sought to enhance the controllability and precision of text-driven motion generation. Some approaches leverage large language models (LLMs) to produce more detailed texts, while others incorporate global 3D coordinate sequences as additional control signals. However, the former often introduces misaligned details and lacks explicit temporal cues, and the latter incurs significant computational cost when converting coordinates to standard motion representations. To address these issues, we propose FineXtrol, a novel control framework for efficient motion generation guided by temporally-aware, precise, user-friendly, and fine-grained textual control signals that describe specific body part movements over time. In support of this framework, we design a hierarchical contrastive learning module that encourages the text encoder to produce more discriminative embeddings for our novel control signals, thereby improving motion controllability. Quantitative results show that FineXtrol achieves strong performance in controllable motion generation, while qualitative analysis demonstrates its flexibility in directing specific body part movements.

1 Introduction

Human motion generation (Guo et al. 2020; Harvey et al. 2020; Song et al. 2021; Chen et al. 2023; Jiang et al. 2023) has become an essential task for various applications such as animation and digital humans. Recent advancements (Guo et al. 2022b,a; Zhang et al. 2024; Tevet et al. 2023; Guo et al. 2024; Tan et al. 2024; Wang et al. 2025a) have shown impressive capability in synthesizing diverse and realistic human motions from given texts, as illustrated in Fig. 1(A). As the quality of generated motions improves, there is a growing demand for generating motions that are not only realistic but also **precise** and **controllable**. Existing works to address these demands fall into two main categories.

On the one hand, some methods (Kalakonda, Maheshwari, and Sarvadevabhatla 2023; Huang et al. 2024; Wang et al. 2025c) leverage detailed textual descriptions to generate precise motions, as shown in Fig. 1(B). Specifically, large language models (LLMs) are used to expand the coarse-grained textual annotations (e.g., “A man stands still and he

is playing the violin.”) into descriptions detailing the movements of individual body parts. These expanded fine-grained descriptions are then connected with the original coarse texts to generate motions. However, this approach suffers from several limitations. First, **the expanded descriptions are often not strictly aligned with the ground-truth motions**, as noted in (Wu et al. 2025), and may contain inaccurate information due to LLM bias. Moreover, the expanded descriptions detail all body part movements of the whole motion sequence, **lacking explicit temporal cues**, such as *when to raise a hand*, making it difficult to achieve precise control over motion within specific time intervals. Besides, this **simple connection paradigm provides limited flexibility for temporally localized control**, as shown in Tab. 4.

On the other hand, methods like (Xie et al. 2024; Wang et al. 2024) introduce spatial control signals to improve controllability, as illustrated in Fig. 1(C). Inpainting-based methods (Shafir et al. 2024; Tevet et al. 2023; Karunaratnakul et al. 2023) integrated spatial constraints into the generation process, but struggle to control joints beyond the pelvis due to the use of relative pose representations. Recent methods (Xie et al. 2024; Wang et al. 2024) addressed the above limitations by converting the generated motion to global coordinates, allowing direct comparison with input control signals and using gradient-based error refinement. However, this coordinate transformation **incurs significant computational cost**, and specifying realistic global coordinate sequences is challenging and unintuitive for users, **limiting applicability and scalability**.

To combine the strengths of both categories while addressing their limitations, we propose a novel controllable motion generation framework: FineXtrol—Fine-grained teXt controllable motion generation, as displayed in Fig. 1(D). Instead of relying on spatial coordinate sequences, FineXtrol uses fine-grained textual descriptions of individual body part movements (e.g., “Move your left hand to your left thigh.”) as the control signals. This eliminates the need for coordinate conversion, improving efficiency, and offers better scalability through the more user-friendly form of control. Moreover, our fine-grained textual control signals are sourced from FineMotion (Wu et al. 2025), whose descriptions are explicitly aligned with ground-truth motions and encode explicit temporal information. Besides, rather

*Corresponding author.

Copyright © 2026, Association for the Advancement of Artificial Intelligence (www.aaai.org). All rights reserved.

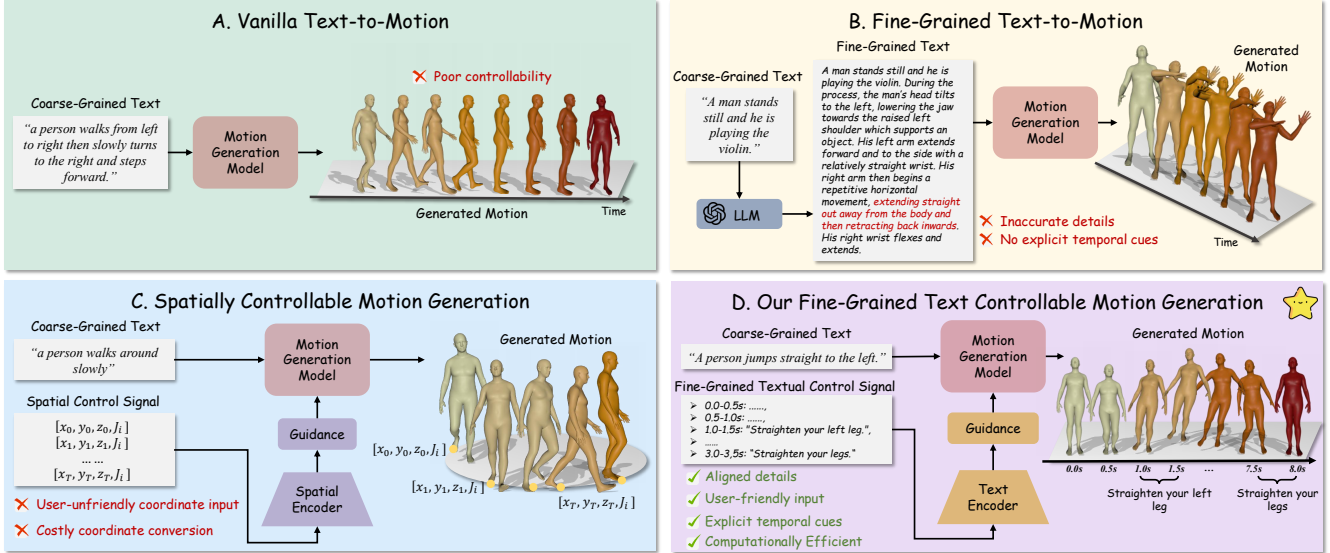


Figure 1: Illustrations of (A) *Vanilla text-to-motion* methods struggle to control specific body part movements. (B) *Fine-grained text-to-motion* approaches using LLMs’ expanded descriptions for fine details, but often misalign with ground-truth motions and lack explicit temporal cues. (C) *Spatially controllable motion generation* methods rely on global 3D coordinate sequences as extra control signals, which are difficult to be provided beyond existing datasets and incur high computational costs from pose conversion. (D) Our *FineXtrol* introduces accurate and temporally explicit fine-grained textual control signals for specific body parts, enabling user-friendly and efficient controllable motion generation.

than directly connecting fine-grained textual control signals with coarse-grained texts as a single input, we incorporate the control signals as residual guidance to modulate the motion features conditioned on coarse-grained texts. These designs lead to the generation of realistic and coherent motions that adhere closely to the specified fine-grained constraints.

During implementation, we observed that widely used text encoders such as CLIP (Radford et al. 2021) and T5 (Raffel et al. 2020) struggle to produce discriminative embeddings for our fine-grained textual control signals, as illustrated in Fig. 7. We attribute this limitation to their pre-training on datasets that emphasize coarse semantics. As a result, these encoders often overlook subtle cues essential for capturing detailed motion semantics. To address this issue, we analyze the characteristics of our fine-grained textual control signals, and introduce a hierarchical contrastive learning module. This tailored module enhances the text encoder’s ability to extract discriminative embeddings for our fine-grained textual control signals, thereby enabling more precise control over human motion generation.

Both quantitative results on HumanML3D (Guo et al. 2022a) and visualizations under various settings demonstrate that our framework, FineXtrol, delivers strong controllable motion generation performance and notably surpasses the previous state-of-the-art in controlling multiple body parts within designated temporal intervals. Moreover, compared with prior diffusion-based controllable motion generation methods, FineXtrol uses fewer trainable parameters and requires less inference time, highlighting the efficiency of our framework. To summarize, our contributions are as follows: **First**, to the best of our knowledge, we propose FineX-

trol, a novel and user-friendly controllable motion generation framework that enables control over body part movements within specific temporal intervals. **Secondly**, we design a hierarchical contrastive learning module to enhance the text encoder’s ability to capture discriminative embeddings for our fine-grained textual control signals, thereby further improving FineXtrol’s capacity to generate motions that accurately follow the specified instructions. **Thirdly**, extensive experiments demonstrate that our FineXtrol excels in precise multi-body-part motion control, and user accessibility, highlighting its potential for real-world applications.

2 Related Work

Text-driven Human Motion Generation. Text-to-motion generation plays a crucial role in various applications. Existing approaches can be broadly categorized into two major generative paradigms (Xie et al. 2024): auto-regressive models (Guo et al. 2022a, 2024; Starke, Mason, and Komura 2022; Rempe et al. 2023; Huang et al. 2024; Juravsky et al. 2022) and diffusion-based models (Tevet et al. 2023; Yuan et al. 2023; Shafir et al. 2024; Karunratanakul et al. 2023; Chen et al. 2023). Auto-regressive approaches generate motion frame-by-frame, while diffusion-based ones progressively denoise an entire motion sequence over multiple iterations. Most of them rely on coarse-grained texts, which often fail to capture the subtle details of human actions. Recent studies (Kalakonda, Maheshwari, and Sarvadevabhatla 2023; Huang et al. 2024; Wang et al. 2025c) have incorporated fine-grained textual descriptions to enhance precise motion generation. However, their LLM-generated detailed texts are often

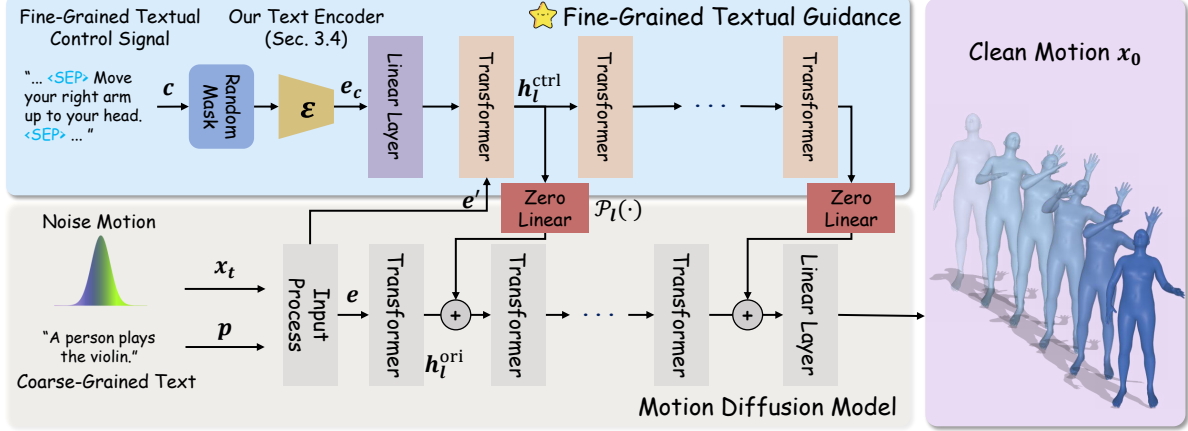


Figure 2: Overview of FineXtrol. Our framework takes the coarse-grained text p , the fine-grained textual control signal c , and a noise motion sequence x_t as input, and predicts the clean motion sequence x_0 . The lower branch resumes from MDM to maintain stable motion generation capabilities from p . The upper branch is a trainable copy of MDM, modulated by c through conditional feature adaptation. The zero-initialized linear layers connect between branches. The framework ensures that the generated motion adheres not only to the coarse-grained text but also to the control signal.

not strictly aligned with ground-truth motions and lack explicit temporal cues, leading to weak correspondence between text and motion segments. This limits control over individual body parts and time intervals. In contrast, our FineXtrol enables precise control over both.

Controllable Motion Diffusion Models. Controllability in diffusion models has been widely studied, especially in image synthesis (Rombach et al. 2022; Ho and Salimans 2022; Zhang, Rao, and Agrawala 2023; Wu et al. 2024), and is now also gaining attention in motion generation area. Inpainting-based methods like PriorMDM (Shafir et al. 2024) condition on observed motion segments to predict missing ones while maintaining global coherence. ControlNet-based methods enhance controllability by injecting conditional signals via a trainable copy of a pre-trained motion generation model. For example, OmniControl (Xie et al. 2024) and InterControl (Wang et al. 2024) use global joint coordinates as control signals, enabling controllability with minimal fine-tuning. However, they require users to provide realistic coordinate sequences, which is impractical, and incur expensive conversions to relative motion representations. Similarly, our method adopts ControlNet paradigm, but employs a more efficient and user-friendly control signal, *i.e.*, fine-grained textual descriptions of body part movements across temporal intervals.

Contrastive Learning for Text Embedding. Learning discriminative sentence embeddings is fundamental to natural language processing. Early methods relied on distributional hypotheses to predict surrounding sentences (Kiros et al. 2015; Logeswaran and Lee 2018; Petrovich, Black, and Varol 2021) or extended Word2Vec with N-Gram representations (Pagliardini, Gupta, and Jaggi 2018). Recent methods have adopted contrastive learning to align augmented sentence pairs (Devlin et al. 2019; Giorgi et al. 2021; Carlson et al. 2021; Yan et al. 2019; Gao, Yao, and Chen 2021).

Contrastive learning has also been effective in multi-modal settings (Wang et al. 2022; Ramesh et al. 2021; Radford et al. 2021; Wang et al. 2025b; Li et al. 2024), aligning image and text embeddings from large-scale paired data. However, most pretrained text encoders focus on coarse semantics and struggle with fine-grained distinctions. To address this, we analyze the properties of our fine-grained textual control signals, and design a contrastive module to extract discriminative embeddings, enabling more precise fine-grained text controllable motion generation.

3 Method

Fig. 2 displays the overall pipeline of our proposed framework, which leverages fine-grained textual descriptions as control signals to guide motion generation. The notations and the definition of this novel research problem are clarified in Sec. 3.1. We then briefly introduce required preliminaries in Sec. 3.2. Next, we detail two key modules in our framework: (1) generating motion sequences guided by our fine-grained textual control signals, which detail specific body part movements in specific temporal intervals (see Sec. 3.3), and (2) representing our fine-grained textual control signals in a robust and discriminant manner (see Sec. 3.4).

3.1 Problem Formulation

Given a coarse-grained text p , such as “*A man kicks something with his left leg*”, and a fine-grained textual control signal c , such as “*Move your left leg to the right in 1.0-1.5s*”, our framework \mathcal{F} should generate a realistic motion sequence $x_0 \in \mathbb{R}^{T \times D}$, where T is the temporal length and D is the dimension of human pose representations. Mathematically, we formulate this fine-grained text controllable motion generation task as:

$$x_0 = \mathcal{F}(p, c; \Theta), \quad (1)$$

where Θ is the parameters of \mathcal{F} .

3.2 Preliminaries

Motion Diffusion Model (MDM) (Tevet et al. 2023) adapted powerful diffusion models to human motion generation by framing the task as a gradual denoising process. Given a ground-truth motion \hat{x}_0 , noise is progressively added to produce a noisy version x_t , where t denotes the number of noise addition steps. Then, conditioned on a time step t and a coarse-grained text p , MDM employed a transformer-based network ϵ_θ with parameters θ to reverse the process and directly predict the clean motion x_0 . The model is trained with the objective function:

$$\mathcal{L}_\theta = \|\epsilon_\theta(x_t, t, p; \theta) - \hat{x}_0\|_2^2. \quad (2)$$

Fine-grained Textual Control Signal c specifies the desired movements of particular body parts within defined temporal intervals. In this paper, we divide the human body into six main parts: *head*, *body*, *left arm*, *right arm*, *left leg*, and *right leg*. See the Appendix for details. An example of a fine-grained control signal for the *right leg* is shown in Fig. 3. Here, `<SEP>` separates the descriptions across different temporal intervals. `<Motionless>` indicates that no movement of the specified body part occurs in that interval.

Move your right leg forward. `<SEP>` Move your right leg back. Point your right foot on the floor. `<SEP>` Move your right leg forward. Bend your right knee. `<SEP>` `<Motionless>` `<SEP>` Move your right leg back.

Figure 3: A fine-grained textual control signal example.

3.3 Motion Generation with Fine-grained Textual Control Signal

To generate human motions that follow coarse-grained texts and the fine-grained textual control signals, we follow the ControlNet (Zhang, Rao, and Agrawala 2023) paradigm to propose a dual-branch framework, as illustrated in Fig. 2. The **lower branch** reuses the original MDM (Tevet et al. 2023) transformer encoder with resumed pretrained weights to ensure stable generation from coarse-grained texts p . Specifically, the “*Input Process*” block includes a CLIP (Radford et al. 2021) text encoder to extract the textual embedding e_p , and linear layers to encode the noisy motion sequence x_t into a motion embedding e_{x_t} . These two embeddings are then concatenated as

$$e = [e_p; e_{x_t}], \quad (3)$$

and fed into the transformer blocks. The output of the l -th transformer block is defined as

$$h_l^{\text{ori}} = \text{TransformerBlock}_l(h_{l-1}^{\text{ori}}), \quad \text{with } h_0^{\text{ori}} = e. \quad (4)$$

Meanwhile, the **upper branch** is a trainable copy of MDM, modulated by the fine-grained textual control signal c through conditional feature adaptation. First, we construct the concatenated textual and motion embedding e' in the same way as the lower branch. To encode the control signal c , we apply random masking on it by replacing descriptions within random temporal intervals with the special token `<Mask>`, and extract its embedding e_c using our

well-designed text encoder (see Sec. 3.4). We then align e_c to the transformer’s embedding space via a linear layer and add it to e' , effectively modulating e' before it is fed into the transformer. The output of the l -th transformer block in the upper branch is computed as:

$$h_l^{\text{ctrl}} = \text{TransformerBlock}_l(h_{l-1}^{\text{ctrl}}), \quad (5)$$

$$\text{with } h_0^{\text{ctrl}} = e' + \text{Linear}(e_c). \quad (6)$$

The upper branch is connected to the lower branch through linear layers $\mathcal{P}_l(\cdot)$ whose weights and biases are initialized to zero. Formally, the interaction between branches at the l -th layer is defined as:

$$h_l^{\text{out}} = h_l^{\text{ori}} + \mathcal{P}_l(h_l^{\text{ctrl}}). \quad (7)$$

This zero-initialization prevents the injection of random noise into the lower branch during the early stages of training. As training progresses, the upper branch gradually learns to interpret the fine-grained textual control signals, capturing both spatial and temporal aspects, and refines the motion by injecting meaningful corrections into the corresponding layers of the motion diffusion model, thereby enhancing motion quality.

3.4 Hierarchical Contrastive Learning for Fine-Grained Textual Control Signal

Commonly used text encoders, such as CLIP (Radford et al. 2021) and T5 (Raffel et al. 2020), exhibit limited capability in extracting discriminative embeddings for fine-grained textual descriptions, especially our fine-grained textual control signals. This limitation hinders the performance of controllable motion generation. To solve this, we analyze the structure of our control signal and identify that it inherently contains three levels of information. As illustrated in Fig. 3:

- The whole example describes a specific body part’s movements across all temporal intervals. Such information is referred to as **sequence-level**.
- Descriptions of a single interval, *i.e.*, between two `<SEP>` tokens, are considered as **snippet-level**.
- Each individual sentence within an interval is defined as **sentence-level**.

Building on this insight, we propose a hierarchical contrastive learning module with level-specific data augmentations to enhance the control signal embeddings. Specifically, we adopt T5 as the base text encoder due to its capacity to encode long text sequences, and progressively train it through contrastive learning at the sentence, snippet, and sequence levels, each initialized from the weights learned at the previous level. Next, we describe data augmentations for each level and the training objective in detail.

Sentence-Level. At this level, the goal is to enable the text encoder to distinguish between different body part movement sentences. Specifically, we build a sentence-level corpus $\mathcal{D}_{\text{sen}}^{\text{ori}}$ with non-repetitive body part movement sentences from FineMotion (Wu et al. 2025), which is the source of our fine-grained textual control signals. Then, we utilize DeepSeek-V2 (DeepSeek-AI 2024) to rewrite each sentence, forming an augmented corpus $\mathcal{D}_{\text{sen}}^{\text{aug}}$ (see Appendix for

prompts). Each sentence in $\mathcal{D}_{\text{sen}}^{\text{ori}}$ and its rewritten counterpart in $\mathcal{D}_{\text{sen}}^{\text{aug}}$ form a positive pair, while all other sentences in the corpora serve as their negative samples.

Snippet-Level. This level aims to make the text encoder robust to the order of sentences within a single time interval. Similarly, we collect snippet-level descriptions from FineMotion to build a snippet-level corpus $\mathcal{D}_{\text{sn}}^{\text{ori}}$. For augmentation, we randomly replace some of the sentences with their counterparts from $\mathcal{D}_{\text{sen}}^{\text{ori}}$ and shuffle their order (see Appendix, Algorithm 1). Each snippet-level description is augmented twice to form a positive pair; augmentations from other snippet-level ones serve as their negative samples.

Sequence-Level. The text encoder in this level aims to enhance its temporal awareness of different temporal intervals’ body part movement descriptions, *i.e.*, our control signals. To construct augmented data at this level, we randomly apply snippet-level augmentations to the individual intervals within a control signal, but preserving the temporal order of intervals (see Appendix, Algorithm 2). Each sequence-level description is augmented twice to form a positive pair, while augmented versions of other sequence-level descriptions are treated as their negative samples.

Contrastive Learning. For all three levels, we train the text encoder with the InfoNCE (van den Oord, Li, and Vinyals 2019) loss, which pulls positive pairs closer and pushes negatives apart. In each minibatch, we sample N original texts and construct positive pairs $\mathcal{c}_i^{\text{aug}}$ and $\mathcal{c}_j^{\text{aug}}$ for each. Their embeddings can be represented as:

$$h_i = \text{Avg}(\mathcal{E}(\mathcal{c}_i^{\text{aug}})), \quad h_j = \text{Avg}(\mathcal{E}(\mathcal{c}_j^{\text{aug}})), \quad (8)$$

where $\mathcal{E}(\cdot)$ is the text encoder, and $\text{Avg}(\cdot)$ denotes the average pooling operation that aggregates the encoder outputs along the sequence length to produce a single embedding. A MLP projection head $g(\cdot)$, randomly initialized for each level, then maps the embeddings into contrastive space:

$$z_i = g(h_i), \quad z_j = g(h_j). \quad (9)$$

Thus, each minibatch yields $2N$ contrastive embeddings in total. Each embedding is contrasted against the other $2(N-1)$ negative ones. The contrastive loss for each embedding, such as $\mathcal{c}_i^{\text{aug}}$, is:

$$\mathcal{L}_i = -\log \frac{\exp(\text{sim}(z_i, z_j) / \tau)}{\sum_{k=1}^{2N} \mathbb{1}_{[k \neq i]} \exp(\text{sim}(z_i, z_k) / \tau)}, \quad (10)$$

where $\text{sim}(\cdot, \cdot)$ denotes cosine similarity, $\mathbb{1}(\cdot)$ is an indicator function, and τ is the temperature parameter.

4 Experiment

4.1 Experimental Setup

Datasets. We conduct experiments on the widely used HumanML3D (Guo et al. 2022a) dataset, using its texts as the coarse-grained texts p . For fine-grained textual control signals c , we use annotations from FineMotion (Wu et al. 2025), which provide detailed body part movement descriptions over short temporal intervals for HumanML3D motions. See the Appendix for details.

Implementation Details. We first progressively train the text encoder across three levels in the hierarchical contrastive learning module, then freeze it to extract control signal embeddings for training our FineXtrol framework. All experiments are conducted on a single A100 40G GPU. We follow the training hyperparameters from (Xie et al. 2024). See the Appendix for detailed hyperparameters.

Evaluation Metrics. The evaluation metrics are categorized into two groups: (1) Generated Motion Quality: Following (Xie et al. 2024), we assess the realism and diversity of generated motions using Frechet Inception Distance (FID), Multi-modal Distance (MM-Dist), R-Precision (Top-1/2/3 motion-to-text retrieval accuracy), and Diversity. For metric definitions, see (Guo et al. 2022a). (2) Textual Representation Quality: To evaluate the discriminability of embeddings for our fine-grained textual control signals, we adopt metrics from (Devlin et al. 2019; Gao, Yao, and Chen 2021), including cosine similarity, alignment, and uniformity. See their papers for details.

4.2 Comparison with State-of-the-arts

We compare different controllable motion generation methods on HumanML3D in Tab. 1. Results in blocks (1)-(3) are taken from (Xie et al. 2024; Wang et al. 2024), while others are our implementations. The implementation details can be seen in the Appendix. From Tab. 1, FineXtrol (*Body Part: Average*) achieves an FID of 0.245 (vs. 0.544) and an R-Top3 of 0.685 (vs. 0.611), compared to MDM without control signals in block (2), which demonstrates the **effectiveness of our novel control framework**. Compared to previous controllable motion generation methods in blocks (4)-(5), FineXtrol achieves state-of-the-art results in R-precision and Diversity, indicating its **ability to generate more diverse and accurate motions**. This supports the advantage of using our precise textual control signals, which offer greater flexibility than rigid spatial coordinates. Moreover, FineXtrol offers a more **user-friendly** approach to guide motion generation. We also compare results on controlling multiple body parts, a more challenging task, in block (6). Specifically, we follow OmniControl to train FineXtrol with combinations of body part control signals, resulting in a total of *i.e.*, $\binom{6}{1} + \binom{6}{2} + \binom{6}{3} + \binom{6}{4} + \binom{6}{5} + \binom{6}{6} = 63$ combinations. During evaluation, one combination is randomly sampled per test instance. Results show that other methods’ *Cross* performance drops significantly, while FineXtrol experiences only

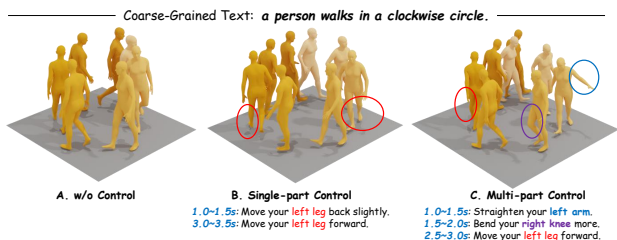


Figure 4: Visualizations of different control settings. $\langle \text{Mask} \rangle$ is used for all unspecified temporal intervals.

No.	Method	Control signal	User-Friendly control	Body Part	FID \downarrow	R-precision \uparrow (Top-3)	Diversity \rightarrow	MM-Dist \downarrow
(1)	Real	-	-	-	0.002	0.796	9.503	2.965
(2)	MDM (Tevet et al. 2023) ICLR’23	-	-	-	0.544	0.611	9.559	5.432
(3)	MDM (Tevet et al. 2023) ICLR’23	Coordinate	×	Pelvis	0.698	0.602	9.197	5.430
	PriorMDM (Shafir et al. 2024) ICLR’24		×		0.475	0.583	9.156	5.424
	GMD (Karunratanakul et al. 2023) CVPR’23		×		0.576	0.665	9.206	5.430
	OmniControl (Xie et al. 2024) ICLR’24		×	Only	0.218	0.687	9.422	4.991
	InterControl (Wang et al. 2024) NeurIPS’24		×		0.159	0.671	9.482	5.026
(4)	InterControl (Wang et al. 2024) † NeurIPS’24	Coordinate	×	Average	0.209	0.684	9.301	5.164
	OmniControl (Xie et al. 2024) † ICLR’24		×		0.255	0.680	9.735	5.054
(5)	CoMo (Huang et al. 2024) † ECCV’24	Text	✓	Average	0.347	0.625	9.568	5.588
	FineXtrol (Ours)		✓		0.245	0.685	9.492	5.087
(6)	OmniControl (Xie et al. 2024) † ICLR’24		×		0.624	0.601	9.334	5.252
	CoMo (Huang et al. 2024)	Text	✓	Cross	0.606	0.611	9.662	5.638
	FineXtrol (Ours)		✓		0.351	0.676	9.658	5.146

Table 1: Quantitative results on the HumanML3D test set. Methods in block (3) are trained with pelvis-only control, while those in blocks (4)-(6) are trained with control over all body parts. *Body Part (Average)* reports the average performance across all body parts under four levels of control signal density: 25%, 50%, 75%, and 100%. *Body Part (Cross)* reports the average performance over the combination of multiple body parts. \dagger refers to our re-evaluation. \rightarrow means closer to real data is better. Results show that our FineXtrol is efficient, user-friendly, and competitive with the existing controllable generation methods. We bold the best results in each block with body part: *Average* and *Cross*.

Body Part	FID \downarrow	R-Top3	Diversity \rightarrow	MM-Dist \downarrow
Head	0.265	0.687	9.423	5.051
Body	0.261	0.679	9.548	5.119
Left Arm	0.224	0.684	9.671	4.981
Right Arm	0.219	0.684	9.427	5.208
Left Leg	0.239	0.685	9.543	5.063
Right Leg	0.263	0.689	9.341	5.100
Average	0.245	0.685	9.492	5.087

Table 2: Detailed results of controlling specific body parts.

a slight decline, highlighting the robustness of our approach.

Following (Xie et al. 2024; Wang et al. 2024), we display the detailed control performance (averaged over all density levels) for six different body parts in Tab. 2. The results indicate that using fine-grained textual control signal of *Right Arm* yields the best FID of 0.219, using those of *Right leg* achieves the highest R-Top3 of 0.689, and using those of *Left Arm* results in the best MM-Dist of 4.981. Detailed results of different control signal densities are provided in the Appendix. We also display our qualitative results in Fig. 4. It shows that FineXtrol supports both single- and multi-part control over different temporal intervals.

Furthermore, we report the inference time and the number of trainable parameters for our FineXtrol and other diffusion-based controllable motion generation models in Tab. 3. Specifically, we calculated the average time required to generate a single motion sequence with 1000 denoising steps, computed over 100 runs on an NVIDIA A100-SMX-40G GPU. The results show that FineXtrol has fewest trainable parameters, and achieves **highest inference efficiency**, benefiting from the absence of conversions between differ-

Methods	Control Signal	Inference Time(s) \downarrow	Params.
OmniControl (Xie et al. 2024)		168.51	48.79M
InterControl (Wang et al. 2024)	Coord.	159.72	42.00M
GMD (Karunratanakul et al. 2023)		153.25	238.63M
FineXtrol (Ours)	Text	128.57	23.39M

Table 3: Inference time and the number of trainable parameters of diffusion-based controllable motion generation methods. ‘Coord.’ is short for coordinate.

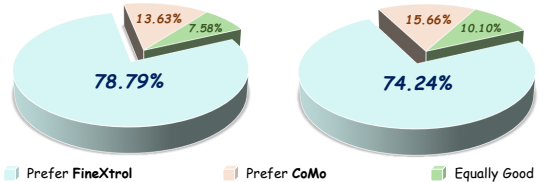


Figure 5: The statistical results of the user study. The *left* pie chart displays the average preference ratio for the visualized motion sequences without fine-grained textual control signals (2 cases) of our FineXtrol and CoMo. The *right* one shows that with fine-grained textual control signals (6 cases). Each case is evaluated based on (1) alignment with control signals and (2) motion naturalness.

ent pose representations.

We also conducted a user study with 33 subjects to compare our method with CoMo, which also uses fine-grained texts to enhance motions. Each subject evaluated 8 cases from two perspectives. According to the statistical results in

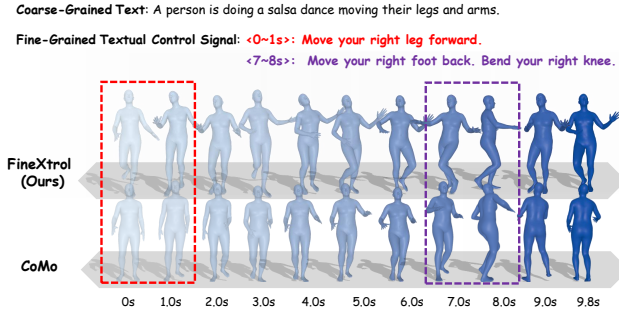


Figure 6: A motion pair comparing *right leg* control in the user study. Body part movements in unspecified intervals are not explicitly controlled.

the *left* part of Fig. 5, our method was preferred over CoMo in 78.79% of the cases without control signals. With control signals (*right* part of Fig. 5), 74.24% of users favored our results. Fig. 6 illustrates a representative example: CoMo produces motions that are misaligned with control signals, whereas FineXtrol yields more faithful and precise motion. More comparisons are provided in the Appendix.

4.3 Ablation Study

We conduct ablation experiments on both the controllable motion generation paradigm and the textual embeddings to validate the effectiveness of our framework’s design choices. We summarize key findings below.

Fine-grained Textual Control Paradigm	FID \downarrow	R-Top3 \uparrow
Direct	1.383	0.601
Ours	0.245	0.685

Table 4: Ablation study on control paradigm. Our control paradigm significantly outperforms the ‘Direct’ paradigm, which directly connects coarse-grained text and fine-grained textual control signals as a single input.

Effectiveness of Our Control Paradigm. We directly connect the fine-grained textual control signals with the coarse-grained text, encode the combined input using our text encoder, following Fig. 1(B), and denote this baseline as ‘Direct’. Tab. 4 indicates that ‘Direct’ control paradigm yields poorer performance, even when the fine-grained descriptions are precise and temporally aware. This suggests that a single-branch model struggles to process densely packed information, and lacks the capacity to fully capture detailed textual semantics. In contrast, our paradigm not only preserves the ability to follow coarse-grained texts but also effectively guides the model to align with fine-grained textual control signals.

Effectiveness of the Hierarchical Contrastive Module for Fine-Grained Textual Control. We compare different text encoders by extracting embeddings for all fine-grained textual descriptions in FineMotion in Fig. 7. Results show

Text Encoder	FID \downarrow	R-Top3	Diversity \rightarrow	MM-Dist \downarrow
CLIP	0.579	0.603	9.310	5.927
T5	0.374	0.659	9.594	5.483
Ours	0.245	0.685	9.492	5.087

Table 5: Ablation study on different text encoders. The controllable motion generation performance with our text encoder significantly surpasses those with CLIP and T5, proving the effectiveness of our hierarchical contrastive learning module for fine-grained textual control signals.

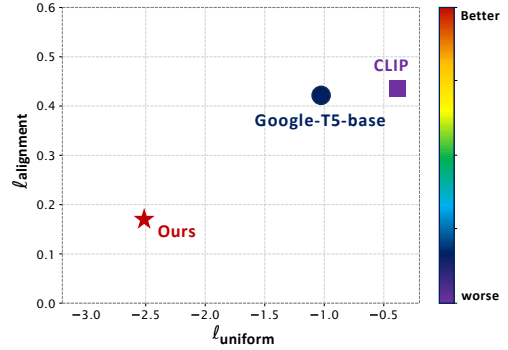


Figure 7: Comparison with existing text encoders in representing fine-grained textual control signals. We plot $\ell_{\text{align}} - \ell_{\text{uniform}}$ of textual embeddings from different text encoders. For both ℓ_{align} and ℓ_{uniform} , lower numbers are better. Results show that our text encoder trained with the proposed hierarchical contrastive learning module performs significantly better than prevalent text encoders.

that our text encoder, trained with the proposed hierarchical contrastive module, yields more discriminative embeddings than prior encoders. More ablations for each contrastive level are provided in the Appendix. We also assess their impact on fine-grained textual controllable motion generation in Tab. 5. Results show that the T5 encoder outperforms CLIP, likely due to CLIP’s truncation of long, detailed texts. With our hierarchical contrastive module, our text encoder achieves further gains, surpassing both T5 and CLIP.

5 Conclusion

In this paper, we propose FineXtrol, an efficient framework that leverages novel and user-friendly control signals, *i.e.*, precise and fine-grained textual descriptions of body part movements, to generate human motion sequences, offering a fresh perspective on controllable motion generation. We further introduce a hierarchical contrastive learning module to enhance the text encoder’s ability to extract discriminative embedding for this novel control signal. Experimental results show that FineXtrol excels in controllable motion generation, particularly in controlling body part combinations. Visualizations further demonstrate its ability to control specific body parts, adjust movements within specific intervals, and manipulate multiple body parts via fine-grained textual descriptions.

6 Acknowledgments

This work was supported by the National Key R&D Program of China (No. 2024YFF0618403), National Natural Science Foundation of China under Grant 62576216, and Guangdong Provincial Key Laboratory under Grant 2023B1212060076.

References

Carlsson, F.; Gyllensten, A. C.; Gogoulou, E.; Hellqvist, E. Y.; and Sahlgren, M. 2021. Semantic Re-tuning with Contrastive Tension. In *9th International Conference on Learning Representations, ICLR 2021, Virtual Event, Austria, May 3-7, 2021*.

Chen, X.; Jiang, B.; Liu, W.; Huang, Z.; Fu, B.; Chen, T.; and Yu, G. 2023. Executing your Commands via Motion Diffusion in Latent Space. In *CVPR*.

DeepSeek-AI. 2024. DeepSeek-V2: A Strong, Economical, and Efficient Mixture-of-Experts Language Model. arXiv:2405.04434.

Devlin, J.; Chang, M.; Lee, K.; and Toutanova, K. 2019. BERT: Pre-training of Deep Bidirectional Transformers for Language Understanding. In *Proceedings of the 2019 Conference of the North American Chapter of the Association for Computational Linguistics: Human Language Technologies, NAACL-HLT 2019, Minneapolis, MN, USA, June 2-7, 2019, Volume 1 (Long and Short Papers)*, 4171–4186.

Gao, T.; Yao, X.; and Chen, D. 2021. SimCSE: Simple Contrastive Learning of Sentence Embeddings. In *Proceedings of the 2021 Conference on Empirical Methods in Natural Language Processing, EMNLP 2021, Virtual Event / Punta Cana, Dominican Republic, 7-11 November, 2021*, 6894–6910.

Giorgi, J. M.; Nitski, O.; Wang, B.; and Bader, G. D. 2021. DeCLUTR: Deep Contrastive Learning for Unsupervised Textual Representations. In *Proceedings of the 59th Annual Meeting of the Association for Computational Linguistics and the 11th International Joint Conference on Natural Language Processing, ACL/IJCNLP 2021, (Volume 1: Long Papers), Virtual Event, August 1-6, 2021*, 879–895.

Guo, C.; Mu, Y.; Javed, M. G.; Wang, S.; and Cheng, L. 2024. MoMask: Generative Masked Modeling of 3D Human Motions. In *IEEE/CVF Conference on Computer Vision and Pattern Recognition, CVPR 2024, Seattle, WA, USA, June 16-22, 2024*, 1900–1910.

Guo, C.; Zou, S.; Zuo, X.; Wang, S.; Ji, W.; Li, X.; and Cheng, L. 2022a. Generating diverse and natural 3d human motions from text. In *CVPR*.

Guo, C.; Zuo, X.; Wang, S.; and Cheng, L. 2022b. Tm2t: Stochastic and tokenized modeling for the reciprocal generation of 3d human motions and texts. In *ECCV*.

Guo, C.; Zuo, X.; Wang, S.; Zou, S.; Sun, Q.; Deng, A.; Gong, M.; and Cheng, L. 2020. Action2motion: Conditioned generation of 3d human motions. In *ACM MM*.

Harvey, F. G.; Yurick, M.; Nowrouzezahrai, D.; and Pal, C. 2020. Robust motion in-betweening. *ACM Transactions on Graphics (TOG)*.

Ho, J.; and Salimans, T. 2022. Classifier-free diffusion guidance. *arXiv preprint arXiv:2207.12598*.

Huang, Y.; Wan, W.; Yang, Y.; Callison-Burch, C.; Yatskar, M.; and Liu, L. 2024. CoMo: Controllable Motion Generation Through Language Guided Pose Code Editing. In *Computer Vision - ECCV 2024 - 18th European Conference, Milan, Italy, September 29-October 4, 2024, Proceedings, Part XXIX*.

Jiang, B.; Chen, X.; Liu, W.; Yu, J.; Yu, G.; and Chen, T. 2023. MotionGPT: Human Motion as a Foreign Language. In *Advances in Neural Information Processing Systems 36: Annual Conference on Neural Information Processing Systems 2023, NeurIPS 2023, New Orleans, LA, USA, December 10 - 16, 2023*.

Juravsky, J.; Guo, Y.; Fidler, S.; and Peng, X. B. 2022. PADL: Language-Directed Physics-Based Character Control. In *SIGGRAPH Asia 2022 Conference Papers*.

Kalakonda, S. S.; Maheshwari, S.; and Sarvadevabhatla, R. K. 2023. Action-GPT: Leveraging Large-scale Language Models for Improved and Generalized Action Generation. In *2023 IEEE International Conference on Multimedia and Expo (ICME)*.

Karunratanakul, K.; Preechakul, K.; Suwajanakorn, S.; and Tang, S. 2023. Guided Motion Diffusion for Controllable Human Motion Synthesis. In *CVPR*.

Kiros, R.; Zhu, Y.; Salakhutdinov, R.; Zemel, R. S.; Urtasun, R.; Torralba, A.; and Fidler, S. 2015. Skip-Thought Vectors. In *Advances in Neural Information Processing Systems 28: Annual Conference on Neural Information Processing Systems 2015, December 7-12, 2015, Montreal, Quebec, Canada*.

Li, Y.; Hou, X.; Dezhi, Z.; Shen, L.; and Zhao, Z. 2024. FLIP-80M: 80 Million Visual-Linguistic Pairs for Facial Language-Image Pre-Training. In *Proceedings of the 32nd ACM International Conference on Multimedia, MM '24, 58–67. Association for Computing Machinery. ISBN 9798400706868*.

Logeswaran, L.; and Lee, H. 2018. An efficient framework for learning sentence representations. In *6th International Conference on Learning Representations, ICLR 2018, Vancouver, BC, Canada, April 30 - May 3, 2018, Conference Track Proceedings*.

Loshchilov, I.; and Hutter, F. 2019. Decoupled Weight Decay Regularization. In *7th International Conference on Learning Representations, ICLR 2019, New Orleans, LA, USA, May 6-9, 2019*.

Mahmood, N.; Ghorbani, N.; Troje, N. F.; Pons-Moll, G.; and Black, M. J. 2019. AMASS: Archive of Motion Capture As Surface Shapes. In *2019 IEEE/CVF International Conference on Computer Vision, ICCV 2019, Seoul, Korea (South), October 27 - November 2, 2019*, 5441–5450.

Pagliardini, M.; Gupta, P.; and Jaggi, M. 2018. Unsupervised Learning of Sentence Embeddings Using Compositional n-Gram Features. In *Proceedings of the 2018 Conference of the North American Chapter of the Association for Computational Linguistics: Human Language Technologies*,

NAACL-HLT 2018, New Orleans, Louisiana, USA, June 1-6, 2018, Volume 1 (Long Papers), 528–540.

Petrovich, M.; Black, M. J.; and Varol, G. 2021. Action-conditioned 3D human motion synthesis with transformer VAE. In *ICCV*.

Radford, A.; Kim, J. W.; Hallacy, C.; Ramesh, A.; Goh, G.; Agarwal, S.; Sastry, G.; Askell, A.; Mishkin, P.; Clark, J.; Krueger, G.; and Sutskever, I. 2021. Learning Transferable Visual Models From Natural Language Supervision. In *ICML*, 8748–8763.

Raffel, C.; Shazeer, N.; Roberts, A.; Lee, K.; Narang, S.; Matena, M.; Zhou, Y.; Li, W.; and Liu, P. J. 2020. Exploring the Limits of Transfer Learning with a Unified Text-to-Text Transformer. *J. Mach. Learn. Res.*

Ramesh, A.; Pavlov, M.; Goh, G.; Gray, S.; Voss, C.; Radford, A.; Chen, M.; and Sutskever, I. 2021. Zero-Shot Text-to-Image Generation. In Meila, M.; and Zhang, T., eds., *Proceedings of the 38th International Conference on Machine Learning, ICML 2021, 18-24 July 2021, Virtual Event*, 8821–8831.

Rempe, D.; Luo, Z.; Peng, X. B.; Yuan, Y.; Kitani, K.; Kreis, K.; Fidler, S.; and Litany, O. 2023. Trace and Pace: Controllable Pedestrian Animation via Guided Trajectory Diffusion. In *CVPR*.

Rombach, R.; Blattmann, A.; Lorenz, D.; Esser, P.; and Ommer, B. 2022. High-Resolution Image Synthesis with Latent Diffusion Models. In *CVPR*.

Shafir, Y.; Tevet, G.; Kapon, R.; and Bermano, A. H. 2024. Human Motion Diffusion as a Generative Prior. In *The Twelfth International Conference on Learning Representations, ICLR 2024, Vienna, Austria, May 7-11, 2024*.

Song, Y.; Sohl-Dickstein, J.; Kingma, D. P.; Kumar, A.; Ermon, S.; and Poole, B. 2021. Score-Based Generative Modeling through Stochastic Differential Equations. In *ICLR*.

Starke, S.; Mason, I.; and Komura, T. 2022. DeepPhase: periodic autoencoders for learning motion phase manifolds. *ACM Trans. Graph.*

Tan, X.; Wang, H.; Geng, X.; and Zhou, P. 2024. Sopo: Text-to-motion generation using semi-online preference optimization. *arXiv preprint arXiv:2412.05095*.

Tevet, G.; Raab, S.; Gordon, B.; Shafir, Y.; Cohen-Or, D.; and Bermano, A. H. 2023. Human Motion Diffusion Model. In *ICLR*.

van den Oord, A.; Li, Y.; and Vinyals, O. 2019. Representation Learning with Contrastive Predictive Coding. *arXiv:1807.03748*.

Wang, H.; Weng, W.; Wang, J.; Zhao, F.; Xie, G.-S.; Geng, X.; and Wang, L. 2025a. Foundation model for skeleton-based human action understanding. *IEEE Transactions on Pattern Analysis and Machine Intelligence*.

Wang, W.; Bao, H.; Dong, L.; Bjorck, J.; Peng, Z.; Liu, Q.; Aggarwal, K.; Mohammed, O. K.; Singhal, S.; Som, S.; and Wei, F. 2022. Image as a Foreign Language: BEiT Pretraining for All Vision and Vision-Language Tasks. *CoRR*.

Wang, X.; Hou, X.; Ding, M.; Chen, J.; Deng, K.; Xie, J.; and Shen, L. 2025b. DisFaceRep: Representation Disentanglement for Co-occurring Facial Components in Weakly Supervised Face Parsing. In *Proceedings of the 33rd ACM International Conference on Multimedia, MM '25*, 4020–4029. Association for Computing Machinery.

Wang, Y.; Li, M.; Liu, J.; Leng, Z.; Li, F. W.; Zhang, Z.; and Liang, X. 2025c. Fg-T2M++: LLMs-augmented fine-grained text driven human motion generation. *International Journal of Computer Vision*, 1–17.

Wang, Z.; Wang, J.; Li, Y.; Lin, D.; and Dai, B. 2024. Inter-Control: Zero-shot Human Interaction Generation by Controlling Every Joint. In *Advances in Neural Information Processing Systems 38: Annual Conference on Neural Information Processing Systems 2024, NeurIPS 2024, Vancouver, BC, Canada, December 10 - 15, 2024*.

Wu, B.; Xie, J.; Ding, M.; Kong, Z.; Ren, J.; Bai, R.; Qu, R.; and Shen, L. 2025. FineMotion: A Dataset and Benchmark with Both Spatial and Temporal Annotation for Fine-Grained Motion Generation and Editing. In *Proceedings of the IEEE/CVF International Conference on Computer Vision (ICCV)*.

Wu, X.; Lai, Z.; Zhou, J.; Hou, X.; Pedrycz, W.; and Shen, L. 2024. Light-aware contrastive learning for low-light image enhancement. *ACM Transactions on Multimedia Computing, Communications and Applications*, 20(9): 1–24.

Xie, Y.; Jampani, V.; Zhong, L.; Sun, D.; and Jiang, H. 2024. OmniControl: Control Any Joint at Any Time for Human Motion Generation. In *The Twelfth International Conference on Learning Representations, ICLR 2024, Vienna, Austria, May 7-11, 2024*.

Yan, S.; Li, Z.; Xiong, Y.; Yan, H.; and Lin, D. 2019. Convolutional sequence generation for skeleton-based action synthesis. In *ICCV*.

Yuan, Y.; Song, J.; Iqbal, U.; Vahdat, A.; and Kautz, J. 2023. Physdiff: Physics-guided human motion diffusion model. In *ICCV*.

Zhang, L.; Rao, A.; and Agrawala, M. 2023. Adding conditional control to text-to-image diffusion models. In *ICCV*.

Zhang, M.; Cai, Z.; Pan, L.; Hong, F.; Guo, X.; Yang, L.; and Liu, Z. 2024. MotionDiffuse: Text-Driven Human Motion Generation With Diffusion Model. *IEEE Trans. Pattern Anal. Mach. Intell.*

A More Details on FineXtrol

A.1 Pseudo-code of Data Augmentation

This section details our data augmentation algorithms for the snippet-level and sequence-level information of the fine-grained textual control signal introduced in Sec. 3.4.

The snippet-level augmentation procedure is presented in Alg. 1. Given a snippet-level description $c_{\text{sni}}^{\text{ori}}$ from the corpus $\mathcal{D}_{\text{sni}}^{\text{ori}}$, we randomly replace some sentences with counterparts from $\mathcal{D}_{\text{sni}}^{\text{ori}}$ and shuffle their order. The modified sentences are then connected to form the augmented snippet-level description $c_{\text{sni}}^{\text{aug}}$. Each snippet-level description is augmented twice to form a positive pair.

The sequence-level augmentation procedure is formalized in Alg. 2. It takes as input a sequence-level description $c_{\text{seq}}^{\text{ori}}$, which consists of an ordered list of snippet-level descriptions. We first split $c_{\text{seq}}^{\text{ori}}$ using the special token $\langle \text{SEP} \rangle$ into individual snippet-level descriptions, apply snippet-level augmentation to each of them, and then concatenate the augmented snippet-level descriptions in their original temporal order using $\langle \text{SEP} \rangle$ to reconstruct the sequence-level description. Similarly, each sequence-level description is augmented twice to form a positive pair.

Algorithm 1: Data Augmentation for Snippet-Level

Input: $\mathcal{D}_{\text{sni}}^{\text{aug}}$: augmented sentence-level corpus
Input: $c_{\text{sni}}^{\text{ori}} \in \mathcal{D}_{\text{sni}}^{\text{ori}}$: a snippet-level description
Output: An augmented snippet-level description $c_{\text{sni}}^{\text{aug}}$

```

1: procedure SNTAUG( $c_{\text{sni}}^{\text{ori}}$ )
2:    $\ell_{\text{sni}} \leftarrow \text{Split}(c_{\text{sni}}^{\text{ori}})$  // Split it into a list of sentences
3:   for each sentence  $c_{\text{sni}}^j \in \ell_{\text{sni}}$  do
4:     if  $\text{rand}() < 0.5$  then
5:        $c_{\text{sni}}^j \leftarrow \mathcal{D}_{\text{sni}}^{\text{aug}}[\text{index\_of}(c_{\text{sni}}^j)]$ 
6:     end if
7:   end for
8:    $\ell_{\text{sni}} \leftarrow \text{Shuffle}(\ell_{\text{sni}})$  // Randomly shuffle sentences
9:    $c_{\text{sni}}^{\text{aug}} \leftarrow \text{'join}(\ell_{\text{sni}})$  // Connect sentences
10:  return  $c_{\text{sni}}^{\text{aug}}$  // Augmented snippet-level description
11: end procedure

```

Algorithm 2: Data Augmentation for Sequence-Level

Input: $c_{\text{seq}}^{\text{ori}}$: a sequence-level description
Output: An augmented sequence-level description $c_{\text{seq}}^{\text{aug}}$

```

1: procedure SEQAUG( $c_{\text{seq}}^{\text{ori}}$ )
2:    $\ell_{\text{sni}} \leftarrow \text{Split}(c_{\text{seq}}^{\text{ori}})$  // Split it into a list of snippets
3:   for each snippet  $c_{\text{sni}}^i \in \ell_{\text{sni}}$  do
4:      $c_{\text{sni}}^i \leftarrow \text{SNTAUG}(c_{\text{sni}}^i)$  // Algorithm 1
5:   end for
6:    $c_{\text{seq}}^{\text{aug}} \leftarrow \text{'<SEP>'}.\text{join}(\ell_{\text{sni}})$  // Connect snippets
7:   return  $c_{\text{seq}}^{\text{aug}}$  // Augmented sequence description
8: end procedure

```

A.2 Prompt for paraphrasing

In Sec. 3.4, we construct an augmented sentence-level corpus $\mathcal{D}_{\text{sen}}^{\text{aug}}$. Specifically, we employ the large language model, DeepSeek-V2 (DeepSeek-AI 2024), to paraphrase each sentence in the original corpus $\mathcal{D}_{\text{sen}}^{\text{ori}}$. Here, we display the prompt used for this paraphrasing task is shown in Fig. 8.

Please paraphrase the given body part movement sentence, while keeping the body part unchanged.

Figure 8: The prompt for paraphrasing sentence-level descriptions.

A.3 Detail of Body Parts Division

OmniControl (Xie et al. 2024) considers six key joints—pelvis, left foot, right foot, head, left wrist, and right wrist—based on their frequent involvement in interactions with objects and the surrounding environment. These joints effectively divide the human body into six main parts. To align with this protocol, we analyze all descriptions about body parts mentioned in fine-grained annotations of FineMotion (Wu et al. 2025) and observe that the descriptions in FineXtrol feature more diverse references: some descriptions target individual joints, while others involve multiple joints. For consistency in evaluation, we also group body parts into six main parts, following the same division strategy. These main parts, along with their corresponding descriptions, are listed in Tab. 6.

Body Parts	Related Descriptions
Head	head
Body	body, torso, waist, upper back, lower back
Left Arm	left hand, left arm, left elbow, left shoulder, left forearm, hands, arms, elbows, shoulders, forearms
Right Arm	right hand, right arm, right elbow, right shoulder, right forearm, hands, arms, elbows, shoulders, forearms
Left Leg	left leg, left foot, left knee, left heel, legs, feet, knees, heels
Right Leg	right leg, right foot, right knee, right heel, legs, feet, knees, heels

Table 6: Controllable body parts and related descriptions.

A.4 Data Augmentation Examples for Three Levels of Information in Fine-Grained Textual Control Signals

As introduced in Sec.3.4, the fine-grained control signal c comprises three levels of information. The data augmentation strategies for each level are detailed in Sec.3.4 and Sec. A.1. Here, we display examples of three levels of descriptions along with their augmented version in the table below.

Table 7: Examples of data augmentation for three levels of information in fine-grained textual control signals.

B More Experimental Details and Results

B.1 Details of Datasets

We conduct experiments on the widely-used **HumanML3D** (Guo et al. 2022a) dataset, which comprises 14,616 motion sequences from AMASS (Mahmood et al. 2019) and HumanAct12 (Guo et al. 2020), along with 44,970 textual descriptions. These textual descriptions serve as the coarse-grained text p .

For the fine-grained control signals c , we use the **FineMotion** (Wu et al. 2025) dataset, which extends HumanML3D by providing fine-grained textual descriptions for all body parts across **420,968** short motion snippets. We extract descriptions of specific body parts to serve as the fine-grained control signals.

B.2 More Implementation Details

Model details. As shown in Fig.2, our model comprises two branches that are fine-tuned jointly. Each branch contains 8 layers of Transformer encoders with a latent dimension of 512. The entire framework has a total of 183M parameters. The encoded feature of our fine-grained textual control signals, e_c , has a dimensionality of $C = 768$.

Training details. The training process consists of two stages. In the first stage, we train the text encoder using a hierarchical contrastive learning module to encode fine-grained textual control signals into discriminative embeddings. In the second stage, we train the entire FineXtrol framework, initializing the text encoder with the weights obtained from the previous stage and keeping it frozen throughout.

When training the text encoder, we adopt T5 (Raffel et al. 2020) as the base text encoder due to its capacity to encode long text sequences. The encoder is progressively trained using contrastive learning at the sentence, snippet, and sequence levels, with each level initialized from the weights learned at the previous one. The same set of hyperparameters is used across all three levels. Specifically, we use the AdamW optimizer (Loshchilov and Hutter 2019) and a batch size of 64. Notably, for long sequence-level inputs, we use a batch size of 16 with gradient accumulation over 4 steps to maintain an effective batch size of 64. The learning rate follows a linear warm-up for the first 1500 iterations, remains constant at 1×10^{-5} , and then decays following a cosine annealing schedule. Each level of contrastive learning is trained for 200 epochs.

For training FineXtrol, we follow the hyperparameter settings of OmniControl (Xie et al. 2024). We use the AdamW optimizer with a learning rate of 1×10^{-5} and a batch size of 64, adopting the total number of training iterations, which is set to 400K (approximately 40 hours on a single A100 40G GPU).

Our framework is trained with 1000 diffusion steps and a cosine noise schedule. Following the classifier-free guidance technique (Ho and Salimans 2022), we randomly mask 10% of the coarse-grained texts p during training. To encode the control signal c , as described in Sec. 3.3, we randomly replace descriptions within temporal intervals with the special token $\langle \text{Mask} \rangle$ at a probability of 50%.

B.3 Comparison with CoMo

We note that CoMo (Huang et al. 2024) also incorporates fine-grained textual descriptions to generate precise motion sequences. Specifically, it defines 10 different body parts (head, torso, left/right arm, left/right hand, left/right leg, left/right foot) plus one additional category for overall mood. Then, it leverages LLMs to generate detailed descriptions for each part. These descriptions are then encoded using the CLIP (Radford et al. 2021) text encoder to produce an 11×512 feature embedding for each motion sequence: 10×512 for the detailed body parts and 1×512 for the mood embedding. The embeddings are flattened and concatenated with the embedding of the coarse-grained text before being fed into the motion generation model.

However, as discussed in Sec. 1 of our main paper, its LLM-generated descriptions suffer from two key limitations: (1) they are not always aligned with the ground-truth motion, and (2) they lack explicit temporal cues, resulting in weak correspondence between the text and motion segments. These issues limit the controllability over both joint movements and temporal intervals. To highlight the strengths of our fine-grained control signals, we conduct extensive qualitative and quantitative experiments.

For fair comparisons, we first map CoMo’s 10 body parts to the 6 body parts used in our control framework, as detailed in Tab. 8.

Body Parts in FineXtrol	Body Parts in CoMo
Head	head
Torso	Torso
Left Arm	L-Arm, L-Hand
Right Arm	R-Arm, R-Hand
Left Leg	L-Leg, L-Feet
Right Leg	R-Leg, R-Feet

Table 8: Conversions of body parts in FineXtrol and CoMo.

Quantitative Comparison with CoMo. Notably, CoMo focuses on precise motion generation rather than controllable motion generation. To evaluate its controllability, we set the textual embeddings of uncontrolled body parts to zero vectors and randomly replace textual embeddings of uncontrolled parts with zero vectors at probabilities of 0%, 25%, 50%, and 75%, aligning with our masking strategy for fine-grained textual control signals. This alignment allows us to quantitatively assess CoMo’s controllable generation performance on each of our six defined body parts, providing a direct and fair benchmark for comparison.

In Sec. 4.2, we report the average performance of controlling different body parts under four levels of control signal density for FineXtrol and CoMo in Tab.1 in the main paper. Results show that our FineXtrol demonstrates a notable advantage in motion quality and text-motion alignment. These results suggest that CoMo is unable to provide precise control signals to a single body part and its performance degrades when control is isolated to specific body parts via masking. Here, we further provide the detailed results of CoMo for each body part across the four levels of control

Density of Control Signal	Body Part	FID ↓	R-precision ↑ (Top-3)	Diversity → 9.503	MM-Dist ↓
25%	Head	0.354	0.625	9.987	5.915
50%		0.351	0.616	9.591	5.811
75%		0.328	0.625	9.405	5.749
100%		0.360	0.632	9.339	5.694
25%	Body	0.363	0.625	9.586	5.905
50%		0.382	0.613	9.213	5.894
75%		0.331	0.631	9.603	5.530
100%		0.345	0.621	9.253	5.501
25%	Left Arm	0.371	0.627	9.732	5.505
50%		0.367	0.619	9.447	5.506
75%		0.335	0.633	9.345	5.477
100%		0.347	0.635	9.416	5.484
25%	Right Arm	0.351	0.627	9.847	5.574
50%		0.352	0.615	9.854	5.530
75%		0.311	0.623	9.801	5.494
100%		0.306	0.633	9.502	5.469
25%	Left Leg	0.356	0.622	9.713	5.517
50%		0.355	0.620	9.387	5.515
75%		0.324	0.626	9.533	5.495
100%		0.345	0.632	9.657	5.512
25%	Right Leg	0.367	0.617	9.636	5.533
50%		0.349	0.620	9.671	5.524
75%		0.331	0.633	9.577	5.480
100%		0.348	0.629	9.534	5.488

Table 9: The detailed controllable motion generation results of CoMo on HumanML3D.

This is my detailed body part movement description for the **head**:
 <Motionless> <SEP> <Motionless> <SEP> Turn your head to the left. <SEP> <Motionless> <SEP> <Motionless> <SEP> <Motionless> <SEP> <Motionless> <SEP> Turn your head to the left. <SEP> <Motionless>

Notably:
 (a) <Motionless> means no body part movements happen in a single temporal interval.
 (b) The descriptions between two <SEP> tokens define a temporal interval with a duration of 0.5s.

Below are some examples of CoMo style for the **head**:

1. The head stays upright, looking forward with a steady pace.
2. The head is held upright, with sharp, quick movements from side to side mimicking the rhythm of the motion.
3. The head remains level and steady, turning slightly as the person looks at the object they need to pick up and the place where they need to wipe.
4. The head remains upright, subtly swaying side to side in alignment with the torso.

Now, I want you to rewrite my detailed body part movements descriptions into CoMo style.

Figure 9: Prompting template for converting our fine-grained textual control signals into the fine-grained description style used in CoMo.

density in Tab. 9.

Qualitative Comparison with CoMo. We displayed more qualitative comparisons with CoMo—also used in our user study (see Sec.B.7)—focusing on the control of body part movements within specific temporal intervals, as shown

Our Fine-Grained Textual Control Signal:

<Motionless> <SEP> <Motionless> <SEP> Turn your head to the left. <SEP> <Motionless> <SEP> <Motionless> <SEP> <Motionless> <SEP> <Motionless> <SEP> Turn your head to the left. <SEP> <Motionless>

CoMo’s Style:

The head remains level and motionless, then smoothly pivots to the left, holding that position briefly before returning to stillness; after a short pause it again turns gently to the left and finally settles back into a neutral, stationary posture.

Figure 10: An example of rewritten fine-grained textual control signal in CoMo’s style.

in Fig.11. As we mentioned before, the LLM-augmented fine-grained descriptions lack explicit temporal cues. To ensure a fair comparison, we rephrase our fine-grained textual control signals to match CoMo’s descriptive style. This is achieved using GPT-4o with a carefully crafted prompt, shown in Fig. 9. The prompt includes several example descriptions from CoMo to guide the LLM in aligning our control signals with CoMo’s format.

Fig.10 shows an example of a rewritten fine-grained textual control signal. We use the CLIP(Radford et al. 2021) text encoder to extract textual embeddings from the rewritten descriptions corresponding to the controlled body part, while setting the embeddings of uncontrolled body parts to

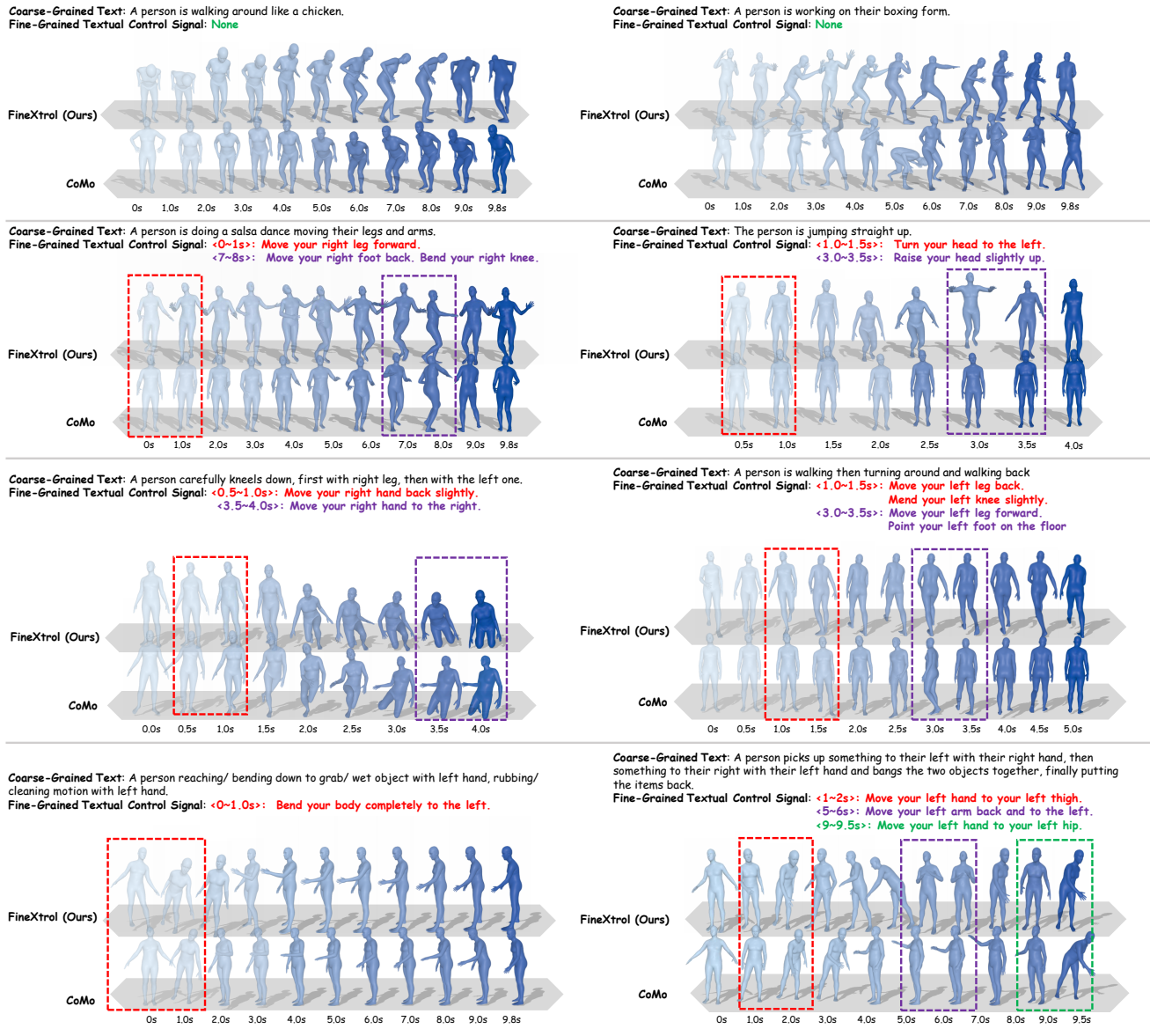


Figure 11: More qualitative comparisons with CoMo. Body part movements in unspecified intervals are not explicitly controlled.

zero vectors. These embeddings are then used to generate controlled motions with CoMo. This setup ensures that the resulting visualizations provide a fair comparison and accurately reflect each model’s capabilities under identical control conditions.

The visualization results in Fig. 11 highlight several key differences between the two models. When using only coarse-grained text, both CoMo and FineXtrol generally produce motions that align well with the input descriptions. However, in scenarios involving more complex or dynamic actions (*e.g.*, *A person is working on their boxing form.*), FineXtrol exhibits a stronger ability to generate vivid and expressive movements. More importantly, when fine-grained textual control signals are introduced within spe-

cific temporal intervals, CoMo’s adherence to the original coarse-grained text often deteriorates. For example, given the coarse-grained text “A person carefully kneels down, first with the right leg, then with the left one,” CoMo mistakenly initiates the movement with the left leg. In general, CoMo struggles with tasks that demand precise control over body parts in designated time intervals, frequently producing motions that are inconsistent with the control instructions. In contrast, FineXtrol reliably executes the specified fine-grained control signals within the correct temporal windows. This observation is further supported by the statistical results from our user study (see Fig. 5 in the main paper), which confirm that FineXtrol provides significantly better fine-grained control over body part movements.

Density of Control Signal	Body Part	FID ↓	R-precision ↑ (Top-3)	Diversity → 9.503	MM-Dist ↓
25%	Head	0.238	0.686	9.424	4.925
50%	Head	0.265	0.683	9.665	4.993
75%	Head	0.297	0.682	9.005	5.119
100%	Head	0.259	0.700	9.597	5.165
25%	Body	0.254	0.649	9.123	5.193
50%	Body	0.239	0.678	9.706	5.108
75%	Body	0.238	0.699	9.900	5.009
100%	Body	0.314	0.690	9.463	5.166
25%	Left Arm	0.305	0.685	9.512	4.823
50%	Left Arm	0.183	0.697	9.681	4.895
75%	Left Arm	0.207	0.659	9.931	5.093
100%	Left Arm	0.203	0.696	9.559	5.111
25%	Right Arm	0.213	0.689	9.592	5.206
50%	Right Arm	0.226	0.654	9.104	5.200
75%	Right Arm	0.239	0.672	9.534	5.224
100%	Right Arm	0.199	0.720	9.477	5.202
25%	Left Leg	0.292	0.672	9.640	5.171
50%	Left Leg	0.181	0.677	9.673	5.020
75%	Left Leg	0.289	0.698	9.305	4.938
100%	Left Leg	0.194	0.692	9.552	5.123
25%	Right Leg	0.258	0.694	9.199	5.163
50%	Right Leg	0.250	0.682	9.500	5.029
75%	Right Leg	0.271	0.696	9.170	5.013
100%	Right Leg	0.273	0.696	9.496	5.195

Table 10: The detailed results of our FineXtrol on HumanML3D.

Density of Control Signal	Joint	FID ↓	R-precision ↑ (Top-3)	Diversity → 9.503	MM-Dist ↓
25%	Pelvis	0.326	0.694	9.783	5.035
50%	Pelvis	0.339	0.690	9.807	5.043
75%	Pelvis	0.350	0.686	9.837	5.051
100%	Pelvis	0.333	0.682	9.876	5.072
25%	Left Foot	0.192	0.688	9.680	5.011
50%	Left Foot	0.216	0.694	9.814	5.020
75%	Left Foot	0.251	0.689	9.789	5.013
100%	Left Foot	0.257	0.681	9.752	5.028
25%	Right Foot	0.178	0.682	9.644	5.027
50%	Right Foot	0.183	0.686	9.730	5.026
75%	Right Foot	0.241	0.690	9.785	5.021
100%	Right Foot	0.212	0.686	9.773	5.026
25%	Head	0.275	0.671	9.660	5.052
50%	Head	0.312	0.669	9.752	5.171
75%	Head	0.318	0.651	9.746	5.050
100%	Head	0.288	0.669	9.766	5.063
25%	Left Wrist	0.184	0.676	9.719	5.013
50%	Left Wrist	0.204	0.685	9.690	5.019
75%	Left Wrist	0.214	0.662	9.711	5.032
100%	Left Wrist	0.236	0.682	9.637	5.033
25%	Right Wrist	0.249	0.677	9.699	5.127
50%	Right Wrist	0.252	0.669	9.658	5.128
75%	Right Wrist	0.253	0.682	9.676	5.130
100%	Right Wrist	0.259	0.671	9.647	5.115

Table 11: The detailed re-evaluation results of OmniControl on HumanML3D.

B.4 Detailed Results for Quantitative Evaluation

We compared two spatially controllable motion generation methods, OmniControl and InterControl, in Tab. 1.(4) of the main paper, as well as the text-controllable CoMo method in Tab. 1.(5), which shares the same control signal modality as our approach. Here, we present the detailed results of a representative spatial control method, OmniControl, along with those of our FineXtrol, to examine the performance trends across different body parts under varying control signal densities. For detailed results of CoMo, please refer to Sec. B.3. To ensure fair comparisons, we re-evaluate OmniControl(Xie et al. 2024) using the same control signal density settings as those employed in our FineXtrol framework, enabling a consistent evaluation protocol across both methods. In this re-evaluation, we retain the use of single-joint control signals, consistent with OmniControl’s original setup. It is important to note that using multiple-joint controls within a single body part can lead to degraded performance, as indicated by the trend observed in Tab. 13.

Interestingly, increasing the control signal density does not always benefit OmniControl—a trend also observed in its original paper. For example, when controlling the ‘Pelvis’ joint, a 100% control density leads to worse performance (FID: 0.3333; Top-3 R-Precision: 0.6816) than using only 25% density (FID: 0.3255; Top-3 R-Precision: 0.6943). A similar trend is observed for the ‘Left Foot’ and ‘Right Foot’ joints, where sparser control yields better FID scores. We attribute this to the challenge of simultaneously satisfying both the coarse-grained text and densely specified global joint coordinate sequences, which impose rigid constraints on the model. Such strict control can hinder the generation of natural motions and weaken alignment with coarse-grained texts.

In contrast, our FineXtrol demonstrates more consistent improvements as control signal density increases. It exhibits a stable upward trend in performance and consistently outperforms OmniControl across most metrics and body parts. We believe this advantage stems from the nature of our fine-grained textual control signals, which are expressed in relative terms and thus allow more flexibility during generation.

Beyond single body part control, we also report the average performance of controlling multiple body parts across all density levels in Tab. 1 of the main paper. Here, we further provide detailed multi-part control results for FineXtrol and OmniControl under the four control densities in Tab. 12 and Tab. 13, respectively. The results echo our earlier observations: as the number of control signals increases, FineXtrol generally improves, while OmniControl tends to degrade.

B.5 More Ablation Study

Effectiveness of the Hierarchical Training in the Proposed Contrastive Learning Module. Fig. 7 in the main paper compares our text encoder—trained with three-level hierarchical contrastive learning—with two widely used encoders, CLIP and T5. In this subsection, we further analyze the impact of each level on the quality of fine-grained textual embeddings, as shown in Tab. 14. Specifically, we use text

Density of Control	FID ↓	R-precision ↑ (Top-3)	Diversity → 9.503	MM-Dist ↓
25%	0.271	0.681	9.681	5.101
50%	0.358	0.677	9.742	5.127
75%	0.428	0.668	9.648	5.177
100%	0.348	0.679	9.560	5.178

Table 12: The detailed results of our FineXtrol for controlling multiple body parts (Cross) on HumanML3D.

Density of Control	FID ↓	R-precision ↑ (Top-3)	Diversity → 9.503	MM-Dist ↓
25%	0.620	0.600	9.297	5.244
50%	0.627	0.604	9.340	5.258
75%	0.616	0.603	9.357	5.249
100%	0.634	0.595	9.342	5.256

Table 13: The detailed re-evaluation results of OmniControl for controlling multiple body parts (Cross) on HumanML3D.

encoders trained with different combinations of contrastive learning levels to extract embeddings for 10,000 randomly sampled positive and negative pairs from each level of textual descriptions. We then compute the average cosine similarity for each group. A more effective encoder for our fine-grained text controllable motion generation task should yield lower cosine similarity for negative pairs and higher similarity for positive pairs, indicating better semantic discrimination. The results demonstrate that applying contrastive learning at a single level (Rows 2–4) enhances the embeddings at the sentence, snippet, and sequence levels compared to the original T5 encoder (Row 1). Further improvements are observed when multiple contrastive learning levels are combined (Rows 5 and 6). Our final encoder, trained with all three levels of hierarchical contrastive learning (Row 6), achieves the best overall performance in capturing fine-grained textual semantics and is therefore adopted as the default in all experiments.

Impact of Hierarchical Contrastive Training on Fine-Grained Text Controllable Motion Generation. We further investigate how different levels of contrastive learning applied to the text encoder affect the controllability of generated motions. Specifically, we evaluate the performance of our fine-grained text-controllable motion generation task using text encoders trained with (i) sentence-level contrastive learning, and (ii) both sentence- and snippet-level contrastive learning, as shown in Tab. 15. The results demonstrate that the encoder trained with (ii) consistently outperforms the one trained with (i) (e.g., FID: 0.409 vs. 0.499). However, both configurations yield significantly lower performance compared to the encoder trained with all three levels, underscoring their limited ability to capture fine-grained textual control signals. These findings highlight the importance of hierarchical contrastive training across all three levels for accurately interpreting fine-grained text and

No.	Level of Contrastive Learning			Sentence level		Snippet level		Sequence level	
	Sentence	Snippet	Sequence	Pos.↓	Neg.↑	Pos.↓	Neg.↑	Pos.↓	Neg.↑
(1)	-	-	-	0.118	0.276	0.100	0.228	0.025	0.235
(2)	✓	-	-	0.110	0.596	0.069	0.446	0.019	0.334
(3)	-	✓	-	0.093	0.589	0.034	0.590	0.012	0.404
(4)	-	-	✓	0.094	0.603	0.045	0.542	0.009	0.407
(5)	✓	✓	-	0.093	0.594	0.033	0.594	0.013	0.384
(6)	✓	✓	✓	0.092	0.625	0.032	0.611	0.008	0.422

Table 14: Ablation study on hierarchical training in the proposed contrastive learning module. We evaluate text encoders trained with different combinations of contrastive learning levels by extracting embeddings for 10,000 randomly sampled positive (Pos.) and negative (Neg.) pairs from each level of textual descriptions, and computing their average cosine similarity. The results indicate that incorporating all three levels of contrastive learning enables the text encoder to best capture the semantics of fine-grained textual descriptions, resulting in better embeddings of our fine-grained textual control signals.

No.	Level of Contrastive Learning			FID ↓	R-Top3 ↑	Diversity →		MM-Dist ↓
	Sentence	Snippet	Sequence			9.503		
(i)	✓	-	-	0.499	0.565	9.919	5.665	
(ii)	✓	✓	-	0.409	0.570	9.858	5.645	
(iii)	✓	✓	✓	0.245	0.685	9.492	5.087	

Table 15: Ablation study on the impact of hierarchical contrastive training. The controllable motion generation performance achieved by our text encoder, hierarchically trained across three levels, significantly outperforms the others, demonstrating the effectiveness of our hierarchical contrastive learning module in capturing fine-grained textual control signals.

generating high-quality motions.

Optimal Temperature and Pooling Methods. Tab.16 investigates the impact of different pooling strategies for textual embeddings $\text{Avg}(\cdot)$ in Equation 8, as well as the effect of the temperature parameter τ in Equation 10. Specifically, we use a text encoder trained with sentence-level contrastive learning to extract embeddings for 10,000 randomly sampled sentence-level positive pairs, and compute their mean cosine distance. The results show that averaging all output tokens from the text encoder yields better performance than using only the first output token as the sentence embedding. Additionally, the best performance—indicated by the smallest cosine distance between positive pairs—is achieved when the temperature is set to $\tau = 0.07$.

Textual Embedding	Temperature τ				
	0.01	0.03	0.05	0.07	0.10
Average token	0.125	0.121	0.112	0.110	0.134
First token	0.208	0.164	0.150	0.148	0.186

Table 16: Ablation study on temperature τ and pooling methods in the proposed contrastive learning module. The results are the average cosine distance between textual embeddings of 10,000 randomly sampled sentence-level positive pairs, where lower values indicate better performance. The results suggest that average pooling yields more effective textual embeddings, and the optimal τ is 0.07.

Masking Prob.	FID ↓	R-Top3	Diversity →	MM-Dist ↓
Varying	0.408	0.560	9.944	5.614
Fixed 0.5	0.245	0.685	9.492	5.087

Table 17: Ablation study on the masking probability in fine-grained textual control signals during training.

Masking Probability in Fine-Grained Textual Control Signals. As described in Sec. B.2, we randomly replace descriptions within temporal intervals with the special token `<Mask>` at a fixed probability of 50% during training. Here, we further investigate the effect of randomly masking these descriptions with *varying* probabilities. As shown in Tab. 17, the *varying* probabilities results in significantly worse motion quality and text-motion alignment. While it yields a slightly higher diversity score, the reduced alignment indicates a lack of control over the generated motions. These results highlight the effectiveness of our fixed 50% masking strategy.

Detailed Results of ‘Direct’ Paradigm. In Sec. 4.3, we investigate replacing our control paradigm with the ‘Direct’ paradigm, which merges the fine-grained textual control signals with the coarse-grained text into a single input. An example of such input is shown in Fig. 12. The average performance of controlling different body parts under four levels of control signal density is reported in Tab. 4 in the main paper. Here, we present the detailed results for each body part under four control density levels in Tab. 18. As the control

Density of Control Signal	Body Part	FID ↓	R-precision ↑ (Top-3)	Diversity → 9.503	MM-Dist ↓
-	-	0.544	0.611	9.559	5.432
25%	Head	1.339	0.581	9.337	4.199
50%		1.391	0.562	9.259	4.397
75%		1.033	0.613	9.045	4.147
100%		1.251	0.593	9.225	4.256
25%	Body	1.044	0.635	9.360	3.929
50%		1.096	0.595	9.456	4.207
75%		0.969	0.619	9.054	4.072
100%		1.002	0.645	9.133	4.151
25%	Left Hand	1.356	0.609	9.241	3.967
50%		1.295	0.606	9.160	4.090
75%		1.197	0.619	9.060	4.027
100%		1.528	0.610	9.265	4.136
25%	Right Hand	1.920	0.608	9.495	4.258
50%		1.968	0.556	9.514	4.421
75%		1.382	0.586	8.941	4.275
100%		1.484	0.605	9.223	4.197
25%	Left Leg	1.216	0.628	9.420	3.903
50%		1.340	0.611	9.151	4.123
75%		1.301	0.612	9.014	4.080
100%		0.940	0.623	9.198	4.087
25%	Right Leg	2.038	0.582	9.506	4.337
50%		2.169	0.558	9.269	4.466
75%		1.449	0.589	9.239	4.298
100%		1.486	0.581	9.225	4.269

Table 18: The detailed results of ‘Direct’ Paradigm on HumanML3D.

signal density increases, the model’s performance on motion generation metrics gradually improves. However, both the FID and MM-Dist degrade notably compared to our FineXtrol method, even performing worse than the original MDM baseline without control signals (Row 1).

A man kicks something or someone with his left leg. <SEP>
<Motionless> <SEP> <Motionless> <SEP> <Motionless> <SEP>
<Motionless> <SEP> Extend your left arm out behind you
<Motionless> <SEP> <Motionless> <SEP> <Motionless> <SEP>
<Mask> <SEP> <Motionless> <SEP> <Motionless> <SEP> Move your
left hand to your left hip. <Motionless> <SEP> <Mask> <SEP>
<Motionless> <SEP> <Motionless> <SEP> <Motionless> <SEP>
<Motionless> <SEP> Move your left hand to your left thigh.

Figure 12: An example input of the ‘Direct’ paradigm. The first sentence is the coarse-grained text, while the underlined sentences indicate the fine-grained textual control signal.

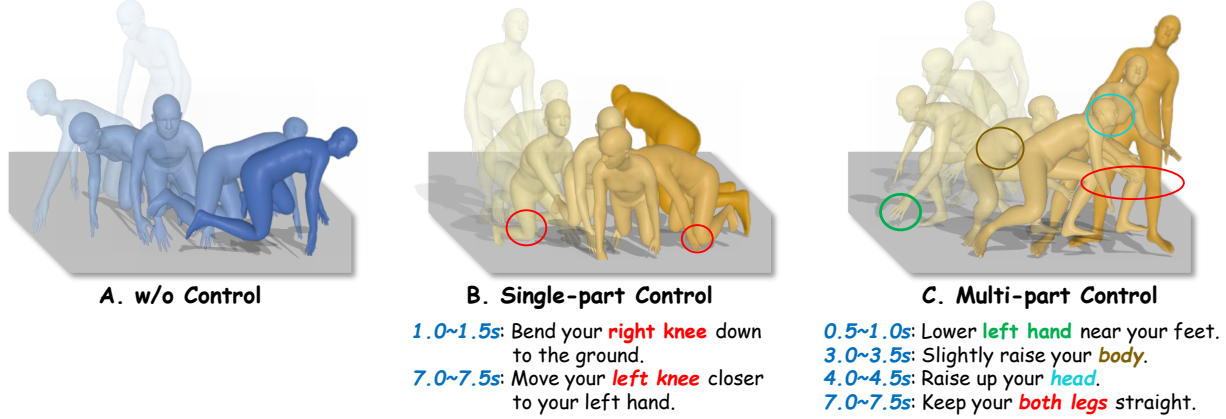
B.6 More Visualization Results

Fig.13 presents additional visualizations of motions generated by our FineXtrol on the HumanML3D (Guo et al. 2022a) test set. From left to right, the columns show generated motions without control signals, with control over a single body part, and with controls over multiple body parts—all conditioned on the same coarse-grained texts.

B.7 Details of User Study

In our user study, we conducted a perceptual evaluation to compare FineXtrol with CoMo (Huang et al. 2024). We generated 8 pairs of 3D motion videos (16 in total) using coarse-grained texts from the HumanML3D (Guo et al. 2022a) test set. These samples cover different fine-grained textual control settings, including 2 examples without control signals and 6 with control signals over different body parts. Participants were shown each video pair and asked to choose the one that better matched both the coarse-grained text and the fine-grained control signals. Fig. 14 illustrates the evaluation instructions and one of the video pairs presented to participants. Full user study are available in the PowerPoint file included in the supplementary materials.

Coarse-Grained Text: *A person acts as a dog on the ground.*



Coarse-Grained Text: *A man raises his arms and lowers them near his waist.*

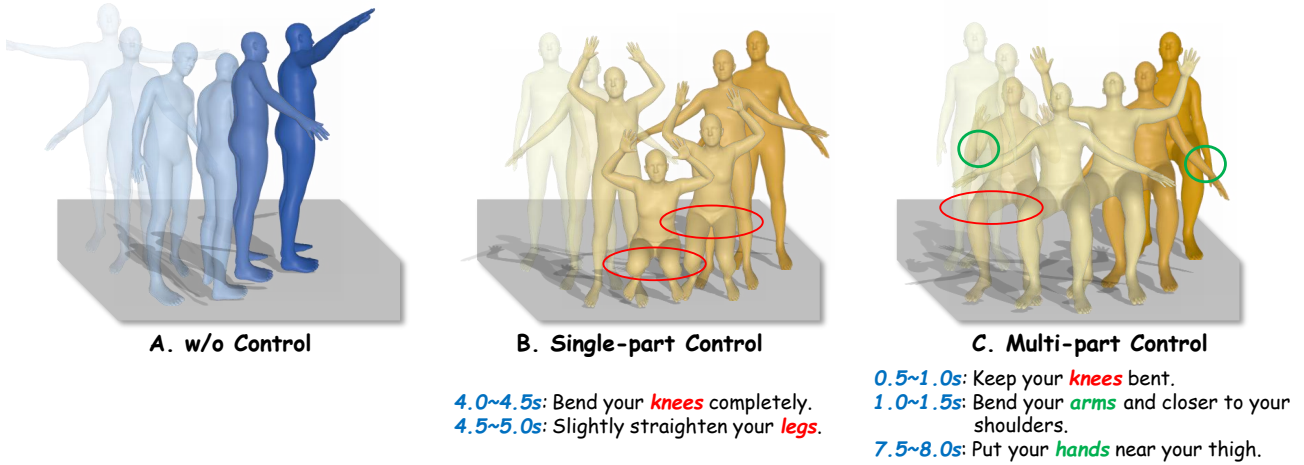


Figure 13: More visualizations of different control settings on the HumanML3D (Guo et al. 2022a) test set. `<Mask>` is used for all unspecified temporal intervals. FineXtrol successfully generates realistic human motions conditioned on various fine-grained textual control signals. Within each sequence, darker colors represent later frames.

User Study for FineXtrol - Instruction

Hi! Thank you for participating in our user study. This will take approximately **5 minutes**.

You'll be presented with **8 pairs** of motion sequences, each accompanied by **a coarse-grained text** and an optional **fine-grained textual control signal**.

For each pair, please choose the motion that:

1. Best matches both the coarse- and fine-grained descriptions.
2. Looks more natural and realistic if both match the descriptions equally well.

Please note:

Text may mention objects (e.g., violins, chairs, balls), but these will not appear in the videos.

Directions like “left,” “right,” and “forward” should be interpreted from the character’s first-person perspective.

Case #1 Coarse-Grained Text: A person is working on their boxing form. Fine-Grained Textual Control Signal: NULL

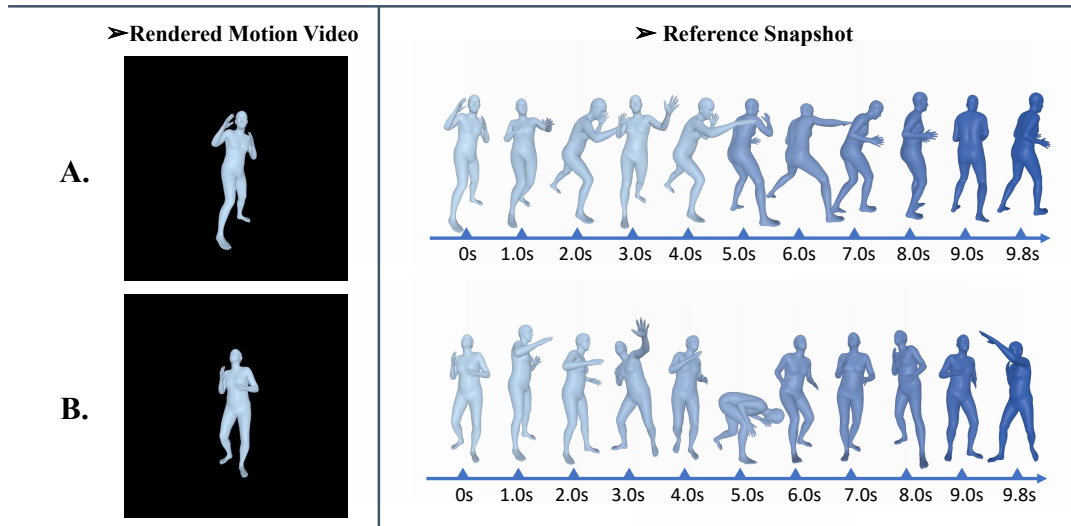


Figure 14: The evaluation instructions and one of the video pairs presented to participants in our user study.